Residual stress analysis in Co-based laser clad layers by laboratory X-rays and synchrotron diffraction techniques

de Oliveira, U.; Ocelik, V.; De Hosson, J. Th. M.

Published in:
Surface & Coatings Technology

DOI:
10.1016/j.surfcoat.2005.12.011

Available online at www.sciencedirect.com
ScienceDirect
Surface & Coatings Technology 201 (2006) 533 – 542
SURFACE & COATINGS TECHNOLOGY
www.elsevier.com/locate/surfcoat

Residual stress analysis in Co-based laser clad layers by laboratory X-rays and synchrotron diffraction techniques

U. de Oliveira, V. Ocelík, J.Th.M. De Hosson *

Department of Applied Physics, The Netherlands Institute for Metals Research, University of Groningen, Nijenborgh 4, 9747 AG Groningen, The Netherlands

Received 23 August 2005; accepted in revised form 2 December 2005
Available online 24 January 2006

Abstract

Thick Co-based coatings were prepared by laser cladding technique on C45 steel substrates with different geometries. Microstructural observations were realized using optical, scanning electron and orientation imaging microscopy. The residual strain state on the surface of a clad layer was determined by the $\sin^2\Psi$-technique using laboratory X-rays. The diffraction of synchrotron radiation in θ–2θ was used to acquire information from the bulk of the materials. Internal stress was characterized through the depth and width of the coatings. Elastic moduli required for stress state calculation were measured by the nanoindentation technique and also estimated from moduli of γ-Co single crystal. A misorientation between principal strain direction and cladding direction was observed on the surface of Stellite 20 coating. The stress profiles inside clad layers reveal the influence of scanning speed, clad layer shape, laser tracks overlap and stress release component due to cross-sectioning. The strong texture inside the coatings affects diffraction conditions, the precision of the measurements and also ability to collect experimental data.

Keywords: Laser cladding; Residual stress; X-rays; Synchrotron radiation

1. Introduction

The laser cladding technique by powder injection is an attractive methodology that allows the deposition of thick protective metallic coatings on softer substrates [1,2]. The process consists of producing a protective layer on the surface of the substrate using a high power laser beam as a heat source while a powder stream is blown under the laser beam. The substrate is scanned by the laser beam that creates a melt pool with a height corresponding to the thickness of a clad. A full coverage of the substrate is attained by the overlap of single tracks. Cracking may occur during or shortly after the laser clad deposition process that is caused by the high residual stresses generated during the solidification stage.

High thermal gradients involved in the process are responsible for the generation of residual stresses, often of harmful tensile nature [3]. During heating the irradiated region expands. However, it is constrained by the cold surrounding area and becomes stressed in compression until melting occurs that relaxes the stresses in the liquid state. It is during the resolidification and cooling down curve that the final stress state is determined. Tensile stresses are formed during shrinkage of the melt pool limited by the metallurgical bonding with the substrate. Clearly, these residual stresses affect the mechanical properties, such as fatigue, creep and brittle fracture behavior.

To improve the quality of a laser deposited clad layer it is essential to characterize the residual stress distribution throughout the clad layer and the effect of the processing parameters, overlapping and geometry of the layer. Stress is an extrinsic property and it cannot be measured directly but only calculated from the experimentally detected displacements converted into elastic strains by using elastic constants.

* Corresponding author.
E-mail address: j.t.m.de.hosson@rug.nl (J.Th.M. De Hosson).

0257-8972/$ - see front matter © 2005 Elsevier B.V. All rights reserved.
doi:10.1016/j.surfcoat.2005.12.011

Existing techniques used for the analysis of residual strains are divided in mechanical and radiation diffraction techniques. Mechanical techniques are destructive and allow analysis of the character, either compressive or tensile. Diffraction techniques, such as X-rays, synchrotron X-rays and neutrons, are non-destructive and open possibilities for a detailed analysis of all components of the strain tensor. The appropriate choice of the adequate radiation and technique depends on sample related features and space resolution required for the measurements [4].

In this work the residual stress state of wear resistant Co–W–Cr (i.e. Stellites) clad layers deposited on C45-steel substrate was investigated. The description of the strain tensor on the surface of the clad was performed by the well-known $\sin^2\Psi$ technique with laboratory Cu-K_α radiation. Mapping of residual stresses was performed on intact and cross-sectioned samples using synchrotron X-ray diffraction analysis. Strong texture was detected in the clad and its effect on the measurements will be discussed. The microstructure, phases and chemical composition of the coating were analyzed by orientation imaging microscopy (OIM), X-ray diffraction (XRD) and energy dispersive X-ray spectrometry (EDS) techniques.

2. Experimental

2.1. Laser cladding: experimental setup and sample characterization

Co–W–Cr alloy powders, Eutrolloy 16012 and Stellite 20, were deposited on C45 low-alloyed steel flat substrates by a computer controlled laser cladding system consisting of powder feeder Sulzer Metco Twin 10C, side and coaxial cladding nozzle, *XYZ*-Rotation CNC table and the 2kW continuous wave Nd:YAG Rofin Sinar laser. The main processing parameters are listed in Table 1. Chemical compositions of the alloying powders and substrate were provided by producers and the compositions of the claddings were determined by EDS analysis (Table 2). The high Fe content of the Stellite 20 sample is caused by the dilution of the steel substrate in the clad when the coaxial cladding nozzle [1] was used.

Table 1
Laser deposited cladding samples and their processing parameters

Description	Powder	Laser Power (W)	Speed (mm/s)	Feeding rate (mg/s)	Nozzle	Substrate
Single track	Eutroloy	1500	5.0	150	Side	Flat
Double track	Eutroloy	1500	5.0	150	Side	Flat
Cladding (9 Tracks)	Eutroloy	1500	5.0	150	Side	Flat
Cladding (9 Tracks)	Eutroloy	1500	6.0	183	Side	Flat
Cladding (9 Tracks)	Eutroloy	1500	5.0	150	Side	Round ∅: 60 mm
Cladding (9 Tracks)	Stellite 20	1200	5.0	133	Coaxial	Flat

Table 2
Chemical composition of powder and substrate (provided by supplier) and cladding layers determined by EDS analysis (wt.%)

Material	C	Si	Cr	Mn	Fe	Co	Ni	W
C45 steel	0.46	0.4	0.4	0.6	Bal.	–	0.4	–
Eutrolloy 16012 powder	1.6	–	29.5	–	–	Bal.	–	8.5
Stellite 20 powder	2.5	1	32	1.5	1.5	Bal.	2.5	17
Clad. Eut. 16012 (5.0 mm/s)	0.2	0.8	28.8	–	1.4	Bal.	–	10.5
Clad. Ste. 20	0.1	1.6	22.4	0.6	31.8	Bal.	1.9	7.8

The phase analysis of Eutroloy 16012 powder and cladding were performed with Cu-K_α and synchrotron diffraction (see Fig. 1). Co-based powders and claddings contained γ-Co and precipitated carbide phases, typical of Co–W–Cr alloys [5]. The measurement performed with Cu-K_α was carried out from a large coating surface area. With synchrotron, this measurement was performed in transmission mode from an irradiated area of approximately $50 \times 1500\ \mu m^2$ at the center of the perpendicular cut of single laser track. The effects of texture are observed as differences in relative peak intensities when the coating is analyzed by these two methods.

The clad layers were on average 1.3 mm thick with 2 mm displacement between the successive tracks. Electron microscopy techniques revealed a dendritic matrix with interdendritic eutectics and average grain size in the order of 100 μm (Figs. 2 and 3). The grains were elongated at the interface of the substrate and changed to bulky shapes on the surface of the clad layer. The residual strains were measured from diffraction data of the γ-Co phase that is located in both the Co-rich primary dendrites and in the eutectic interdendritic phases (see Fig. 3A). As the actual residual stress contains a superposition of macrostresses and microstresses, the shift in diffraction peaks originates from contributions of the γ-Co primary dendrite, which solidifies at first, and γ-Co in eutectic that is formed at a later stage of solidification.

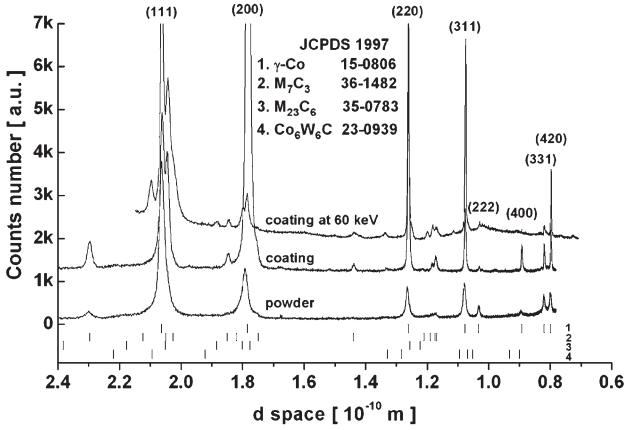

Fig. 1. XRD spectra of Eutroloy 16012 powder and coating analyzed by laboratory Cu-K_α X-ray, $\lambda = 1.5405$ Å, and Synchrotron at 60 keV, $\lambda = 0.206762$ Å.

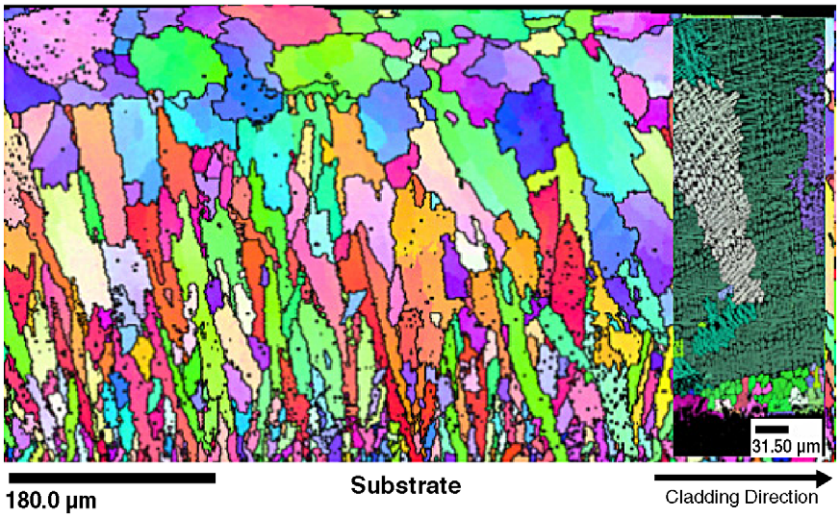

Fig. 2. Orientation Imaging Micrograph of Eutroloy 16012 cladding in a single-track longitudinal section. Detail of dendritic microstructure near the interface with the substrate is shown in the insert.

Field emission gun scanning electron microscopes Philips XL30 and XL30S equipped with EDS and EBSD detectors were used to study the microstructure of the prepared samples. The nanoindentations were performed with MTS Nano Indenter XP.

2.2. Determination of macroscopic elastic constants

The elastic constants required for calculation of internal stress state were found by two different methods: isotropic Young's modulus E of the Co-based cladding was measured by nanoindentation; Young's modulus E and Poisson's ratio ν for (311) planes of the γ-Co phase were calculated from elastic constants of a single grain. The residual stresses were then calculated from the measured strains.

The hardness and Young's modulus of the Eutroloy 16012 cladding were measured by averaging 124 nanoindentions, where the depth of the indents was fixed to 1 µm. As Fig. 3B shows, the size of Berkovich indents is comparable to the size of the γ-Co dendrites. Therefore, the nanoindentation measurements contain contributions from the γ-Co dendritic phase and from the interdendritic eutectic composed of γ-Co and hard carbidic phases. The volume content of dendritic phase in the coating was estimated from Fig. 3A as 55%. However, we will assume that the measured properties describe the isotropic behavior of the material. The averaged values of hardness and elastic modulus are 9.75±1.00 GPa and E_{meas}=286±14 GPa, respectively.

The various components of the stress tensor can also be calculated using elastic constants that take the anisotropy of the cubic system into account. For the evaluation of the elastic constants of polycrystalline multi-phase materials several approaches have been proposed [6–8]. The elastic modulus of γ-Co was calculated applying Hill's approximation [9]. The shift of (311) fcc plane reflection responds almost linearly to loading at the start of the elastic regime [10,11] and therefore it was chosen as a suitable reflection for the characterization of macroscopic strains and stresses in our experiments. The experimental values of coefficients of stiffness C_{11}, C_{12} and C_{44} of pure Co given in [12] were used for the calculations [9] of $E_{Co(311)}$=216 GPa and $\nu_{Co(311)}$=0.3077.

The internal stresses can be then calculated using both, the measured and theoretical, elastic constants.

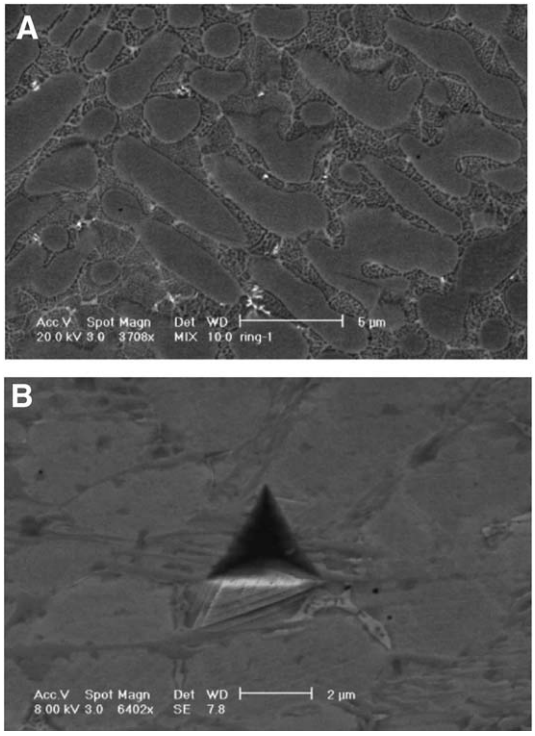

Fig. 3. SEM micrographs: (A) Eutrolloy 16012 cladding microstructure: Co-rich primary dendrites and the eutectic interdendritic space constituted by γ-Co rich phase and hard carbidic phase. (B) nanoindented area presenting shear bands observed in the primary dendrites typical for cobalt alloys.

2.3. Experimental analysis of residual strains: X-ray diffraction experiments

X-ray stress analysis is based on measuring peak shifts due to deformation of the crystal lattice spacing caused by the residual stresses, assuming the elastic regime. Residual stresses appear as a consequence of inhomogeneous deformation. The coordinate systems assumed are given in Fig. 4A. The *X*-axis is placed longitudinally to the cladding direction on the surface plane, the *Y*-axis is in the transversal direction to the cladding direction and the *Z*-axis is vertical to the sample plane.

The attenuation depth of laboratory X-rays into a metal or alloy is usually of the order of few micrometers. For instance 66% absorption of CuK_α in this Stellite 20 cladding occurs below a depth of 4 μm [13]. Since the analyzed volume corresponds to a thin surface layer defined by the irradiated area and penetration depth, the $\sin^2\Psi$ technique assumes that the layer is under a biaxial stress state. When θ–2θ diffraction analysis is performed over a range of side angle Ψ, only grains specifically oriented to this angle Ψ fulfill the Bragg's condition and will diffract. A shift of the diffraction peak due to elastic strain of the crystal lattice can be detected for each Ψ angle. From the measured values of lattice spacing d_Ψ at angle Ψ the strain is defined as:

$$\varepsilon_\psi = \frac{d_\psi - d_0}{d_0}, \tag{1}$$

where d_0 is the lattice spacing of a stress-free grain. This is usually exchanged with $d_{\Psi=0}$, leading to negligible errors [14]. The strain tensor is measured in the crystal reference system (*hkl*) and is transformed to the sample surface reference (*XYZ*) by algebraic operations. It is possible to derive the fundamental equation of strain tensor on the surface of the material in a biaxial stress state using the transformation of a second rank tensor, given by:

$$\begin{aligned}\varepsilon_{\phi\psi} &= \frac{d_{\phi\psi} - d_o}{d_o} \\ &= \left(\varepsilon_{11}\cos^2\phi + \varepsilon_{12}\sin 2\phi + \varepsilon_{22}\sin^2\phi\right) \cdot \sin^2\psi \\ &\quad + (\varepsilon_{13}\cos\phi + \varepsilon_{23}\sin\phi)\sin 2\psi + \varepsilon_{33}\cos^2\psi\end{aligned} \tag{2}$$

where, ϕ represents a rotation angle around an axis *Z* normal to the sample surface. When shear stresses perpendicular to the plane are found, ε_{xz} and $\varepsilon_{yz} \neq 0$ then the so-called $\sin^2\Psi$ splitting is detected. The coordinate system can be transformed so that only principal strains are present and the factor in front of $\sin^2\Psi$ argument in Eq. (2) is canceled.

The X-ray experiments were carried out with a Phillips X'pert X-ray system equipped with a Cu radiation source, $\lambda_{CuK\alpha} = 1.5405$ Å. The family of planes chosen for strain analysis was (311) and side angle Ψ range was from −60° to 60° scanned in three different axis: transversal to laser tracks ($\phi = 0°$), diagonal to laser tracks ($\phi = 45°$) and longitudinal to laser tracks ($\phi = 90°$).

The Stellite 20 clad layer was ground 0.2 mm to eliminate surface roughness after laser cladding, polished and electro-polished to eliminate the surface deformed layer with an electrolyte based on perchloric acid 60 vol.% and ethanol.

Two samples related features cause the low count intensity, which made this experiment time consuming. First is the size of the laser tracks. To avoid any contribution of diffraction from the neighboring track the required spatial resolution was defined by the track width, which is approximately 2 mm. The analyses are performed on the center of the surface of the clad in a squared irradiated area of 2 mm^2 for $\Psi = 0$. Further, the microstructure is coarse grained and a texture was detected through the fluctuation of the peaks intensity for different Ψ angles.

2.3.1. Synchrotron experimental setup

High photon flux and a small beam divergence make synchrotron radiation a relevant technique to measure residual strains non-destructively in depth. The experiments were executed on the powder diffraction Beamline ID-31 of the ESRF-France. The energy was 60 keV selected by Si monochromators, providing a wavelength of 0.206762 Å. For the preparation of the experiment it is important to know the attenuation depth of the radiation into the material, the path length and to describe the gauge volume from where information is acquired.

The samples were single, double and 9-tracks of Eutroloy 16012 clad layers on a flat substrate and a 9-track cladding layer deposited on a 60-mm ∅ round bar. Two scanning modes were applied; in reflection, where intact samples were used, and in transmission on 1-mm thick perpendicular cross-sections prepared by spark erosion cutting. The attenuation depth of

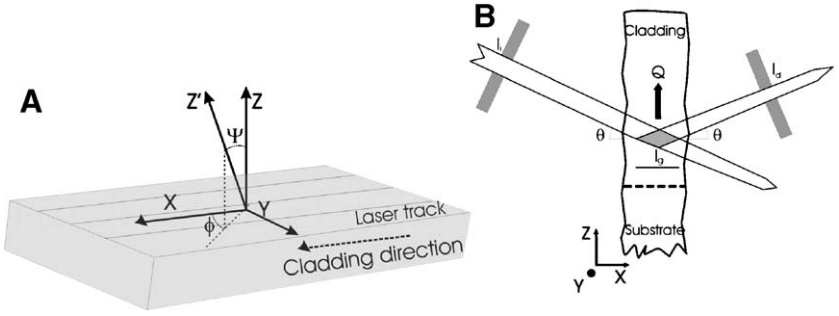

Fig. 4. Schematics showing strain measurement geometry, (A) definition of reference axis system and (B) sampling Gauge volume, where *Q* is the scattering vector, or direction of the measured strain.

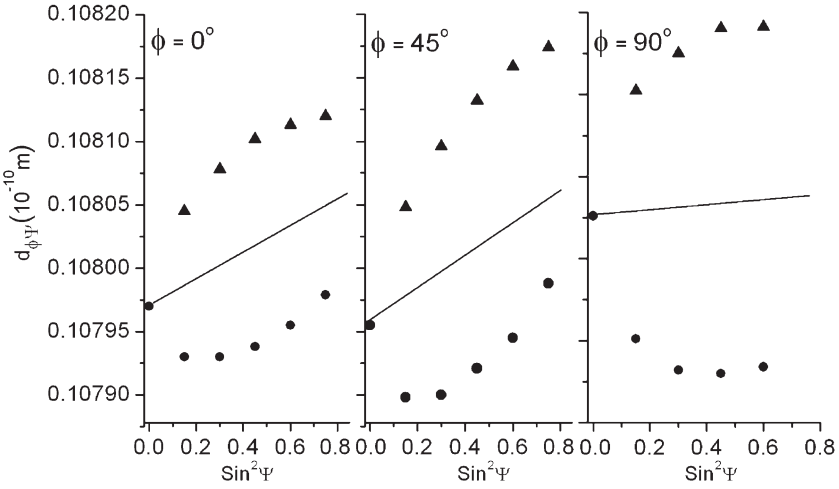

Fig. 5. Plots of $d_{\phi\Psi}$ vs. $\sin^2\Psi$ characterize residual strains along three different directions. The measurements carried out on positive (●) and negative (▲) Ψ's reveal the Ψ-splitting. The linear behavior is obtained by averaging.

66% radiation absorption [13] for a homogeneous finite film is calculated by:

$$I_z = I_0 \cdot e^{(-\mu/\rho)\cdot\rho z} \tag{3}$$

$$(\mu/\rho)_t = \sum_{i=1}^{n} w_i \cdot (\mu/\rho)_i, \tag{4}$$

where I_z is transmitted beam intensity, I_0 is the initial intensity of the beam, z is the film thickness, μ is a proportionality constant and ρ is the density of absorber. (μ/ρ) is the mass absorption coefficient of an element and is tabulated in literature.

For the composition of Eutroloy 16012 cladding (see Table 2), the calculated attenuation length l_μ is 0.875 mm. When synchrotron diffraction experiments are performed in reflection mode, the minimum feasible X-ray path length l_{path} plays an important role in the set-up. The path length is calculated based on the required depth l and the diffraction angle of the chosen peak, according to:

$$l_{path} = 2\left(\frac{l}{\sin\theta}\right). \tag{5}$$

In the case of γ-Co (311) peaks the l_{path} is approximately 18 mm for 1 mm depth.

The spatial resolution along the Z-axis [15,16] is determined by the aperture of the incident and diffracted slits (see Fig. 4B). In our experiments l_i and l_d were fixed to 50 μm. The gauge length, l_g, is calculated from the slits dimensions and diffraction angle θ:

$$l_g = \frac{l_i}{2\sin\theta} + \frac{l_d}{2\sin\theta} \tag{6}$$

The analyzed peak corresponds to the (311) planes, for $\lambda_{60\ keV}$=0.206762 Å the diffraction angle θ is about 5.5° and therefore $l_g \approx 500$ μm. The width aperture in the Y-axis was fixed by the instrument to 1.5 mm, i.e. narrower than the width of the laser track. In conclusion, the residual strains are sampled from a lozenge shaped volume with 50 μm height, 500 μm length and 1.5 mm width from where the beam is diffracted.

3. Results and discussions

3.1. Plane stress tensor components at surface of Stellite 20 clad layers

The $\sin^2\Psi$ method defines the plane stress tensors by the slopes of the graphs and the elastic constants of the material [14]. Fig. 5 presents the change of measured d-spacing as a function of $\sin^2\Psi$ in the longitudinal direction, along the diagonal, and perpendicular to the laser cladding direction. When the residual strains are measured in a coordinate system that does not coincides with the system of the principal stresses, the terms ε_{13} and ε_{23} in Eq. (2) are non-zero and the d-spacings measured at corresponding positive and negative Ψ's will be different. This is also known as Ψ-splitting. Such situation can be observed on Fig. 5. The d_0 used for strain tensor calculation using Eq. (2) was 0.10800 nm.

The stresses were calculated assuming the elastic constants: $E_{Co(311)}$ and $\nu_{Co(311)}$. The stress tensor, σ_{xy}, components lie on the XYZ coordinate system and the principal stresses in the rotated coordinate system, $\sigma_{x'y'}$, was calculated by linear algebra (in MPa):

$$\sigma_{xy} = \begin{pmatrix} 161 & 116 \\ 116 & 137 \end{pmatrix} \quad \text{and} \quad \sigma_{x'y'} = \begin{pmatrix} 266 & 0 \\ 0 & 33 \end{pmatrix}.$$

The surface of the Stellite 20 coating is found under a tensile stress state where the major principal stress is tilted approximately 40° from the cladding direction (Fig. 6A).

One may expect a relation between the orientation of principal stresses and the direction of propagation of solidification front. When a single track is deposited a solidification front on the surface moves with the laser scan direction [17] and the major stress axis is expected to lie along the cladding direction. An overlap of single tracks changes the direction of

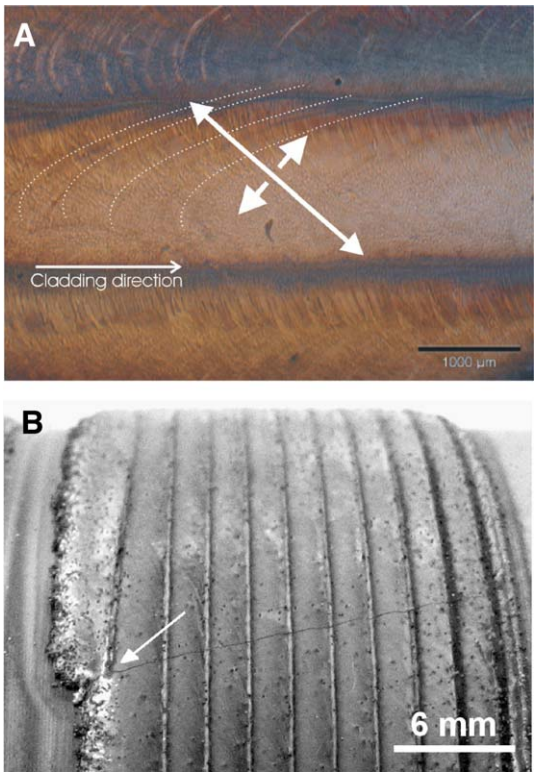

Fig. 6. (A) Principal components of stress tensor at the place of the measurement represented by arrows on the surface in the centre of Stellite 20 cladding on flat substrate. Chemically etched surface reveals microstructure and consequently bands created during solidification are visualized. (B) Cracking formed after the laser cladding of Eutroloy 16012 coating on round steel substrate. Crack initiation site is indicated by arrow.

the solidification front due to modification of the heat transfer boundaries and remelts usually 20–30% of the previous track. Optical microscopy analysis of the etched cladding layer revealed that on the surface the solidification bands lie are inclined to the cladding direction (Fig. 6A). From this observation it is concluded that the major principal stress axis tends to lie perpendicular to the solidification front. Cracking could be observed after cladding experiments when the clad layer reached a height above 1.7 mm. At the location where the laser stops a stress concentration is formed where the crack usually initiates. From thereon, it propagates through the whole coating along a direction perpendicular to the principal stress direction. Fig. 6B shows such crack crated in Eutroloy 16012 coating formed on C45 round substrate. In this case the size of two principal stress components must be close to each other because the crack propagates at a direction, which corresponds to the minor principal stress direction. It should be mentioned that probably the size of a tilt angle between the cladding direction and one principal stress direction will depend on amount of overlapping, height of the coating and also on the scanning speed. We found only one reference in literature, which mentions a rotation of principal stress axes towards cladding direction. Grum and nidaršiè [18] studied the internal stress profiles of clad layers on low carbon steel by the so-called hole drilling method. The two principal residual stress components made a non-specified angle with a reference to the cladding direction. These had a slightly compressive character only at the surface and they changed to tensile ones and increased with depth. Independently of the clad material, the ratio between these components was always close to 2:1. Maximum principal stress component for Stellite 6 clad was found about 450 MPa.

3.2. Influence of parameters in residual strain/stress measurements

The diffraction peak of the (311) family of planes is observed at about $2\theta = 11°$ when the wavelength is 0.206762 Å, that is, in transmission mode the planes are tilted 5° from surface of the clad. For simplification, it is assumed that in all cases the lattice spacings measured are parallel to the specimen top surface. Further, due to the width of the synchrotron beam it is possible to measure the averaged residual strains component inside 1.5 mm as function of depth. The stress free lattice spacing d_0, 1.07846 Å, used for ε_z calculation was measured from a

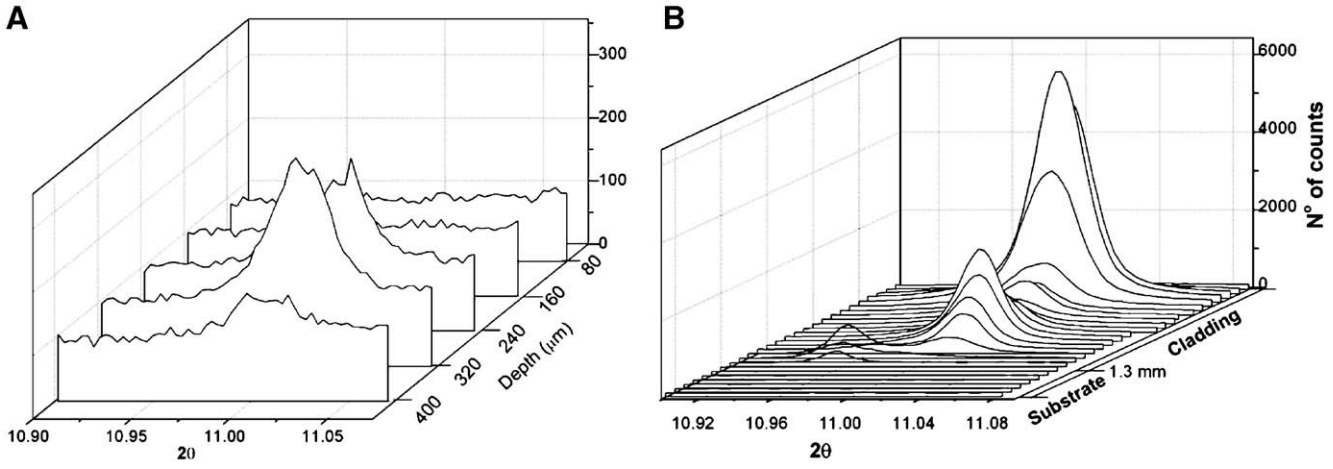

Fig. 7. γ-Co(311) diffraction peaks acquired in depth. The zero depth corresponds to the top of the coating: (A) Intact sample peaks measured in reflection mode. (B) Cross-sectioned sample acquired in transmission mode. Double peaks (at 10.95 and 11.05) are detected close to the interface between cladding and substrate.

single-track cladding that was sectioned using spark erosion cutting of the substrate in order to release the macro-stresses.

When intact samples were scanned in reflection mode the textured microstructure did not allow assessing the residual strain in depths above 0.5 mm and the diffracted beam intensity was very low due to the radiation attenuation over the path length (Fig. 7A). This was observed during alignment experiments when the detector was fixed at the (311) peak position, i.e. $2\theta = 11°$ and the gauge volume was scanned over depth and width. The horizontal scan of gauge volume through the width of the clad (Fig. 8) revealed (311) reflections on the sides of clad track, but due to a texture no diffraction took place in its center. The differences in peak intensities are caused by the attenuation of the incident beam in the material. The lower peaks are therefore observed on the farther side of laser track looking from a position of incoming beam. From the known length of the gauge volume (500 μm) and widths of the peaks on the right side in Fig. 8, it is possible to estimate the thickness of a near surface clad area, which contributes to the diffraction. This quantity varies from 0.2 to 0.3 mm and the shape of these peaks is created by gradual filling of the gauge volume during entering and leaving this area.

In transmission mode, however, it was possible to make a profile of the residual strains through the entire depth of the coatings when the incidence angle was changed (Fig. 7B). Further, the intensity of the diffracted beam was much higher than in reflection mode. The peak positions were defined by Gaussian and Lorenzian fitting with a negligible difference in the fitted values. Close to the interface with the substrate double peaks were detected. Chemical analysis performed by EDS showed an increase in the Fe content at the interface, which may lead to a change of the lattice spacing. Probably the gauge volume irradiates the regions with different Fe contents that cause these double peaks. These peaks were not used for calculation of the residual strain due to lack of d_0 data.

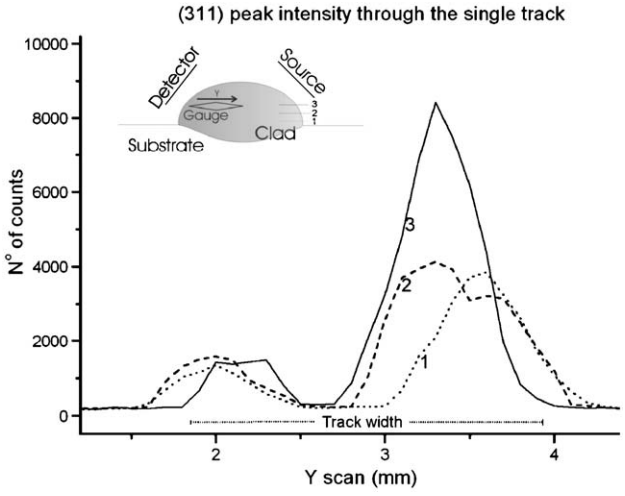

Fig. 8. The (311) peak intensity through the width of single clad track scanned by synchrotron gauge volume. Lines 1, 2 and 3 represent the scans performed at three different heights. In the insert it is demonstrated schematic position of scans. The difference in peak heights is caused by the radiation absorption through the cladding.

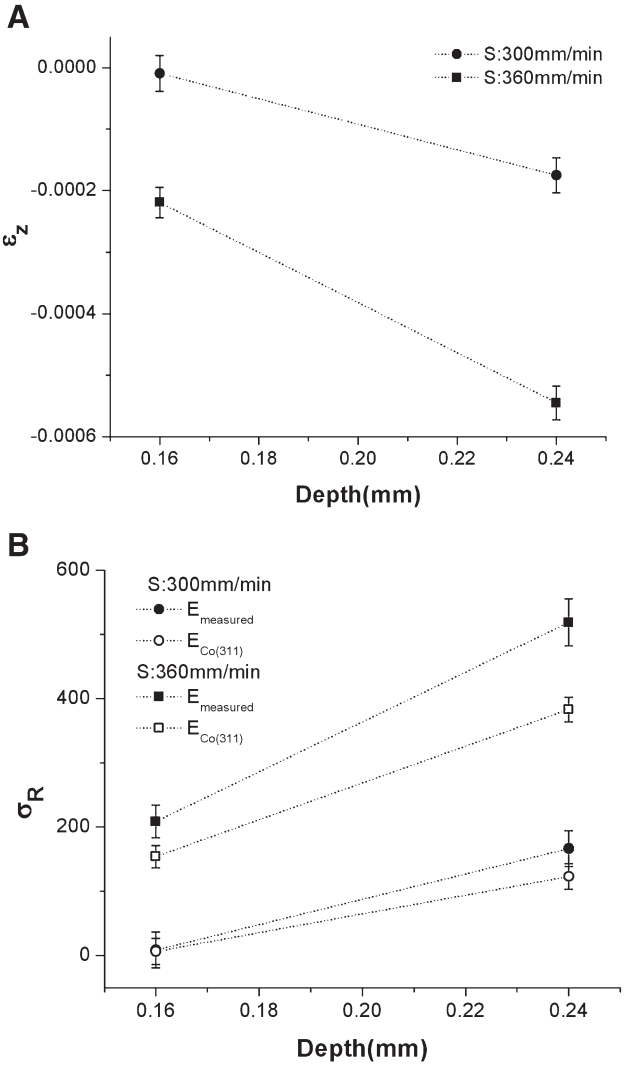

Fig. 9. (A) Residual strains along the vertical axis Z measured on samples deposited at 300 and 360 mm/min. (B) The residual stresses σ_R calculated with the empirical E_{meas} and $E_{Co(311)}$ elastic moduli. Doted lines indicate points that belong to the same depth profile.

It is assumed that the residual strain ε_z is due to the Poisson's contraction caused by the stresses in XY plane, characterized by the first stress invariant $\sigma_R = \sigma_x + \sigma_y$ and it is possible to estimate the nature of the stresses, whenever tensile or compressive. The first stress invariant on the XY plane is then calculated by Hooke's law with the simplified form:

$$\sigma_R = -\frac{E}{v}\varepsilon_z. \tag{7}$$

The experimental errors arise from the errors of measured values of lattice spacing d, d_0 and the experimental E_{meas}. A relative experimental error of the order of 10^{-5} is a typical estimate of synchrotron diffraction peak position. During our experiment the quality of the peaks used for the determination of the (311) lattice spacing varies depending on the local

texture. This is the main source of the error fluctuation in the plots of strain and stress that are presented in Section 3.3. For the residual strains a typical relative error, which covers 95% confidence interval, is about 15%. The error in the stress values increases to 18% when E_{meas} used is obtained from the nanoindentation. When the stresses are calculated from the theoretical $E_{(Co311)}$ the accumulated error is analogous to the residual strain error. Confidence interval of 95% was used in the plots.

3.3. Effects of cladding parameters and residual stress profiles

The residual strains were measured in reflection mode on the central tracks of Eutroloy 16012 claddings deposited at 300 and 360 mm/min scanning speeds (see Fig. 9). The diffraction phenomena took place at the same depths in two different samples, which indicate reproducibility of the grain structure in the clad. In both samples the residual stresses were almost zero at the surface and increased quickly as a function of depth. The highest values are found in the sample deposited at higher scanning speed that generated higher cooling rate. This result is in qualitative agreement with results of Zhou and De Hosson [19], showing with the $\sin^2\Psi$ method that after laser surface remelting of stainless steel substrate both near surface stress components (longitudinal and transversal) are tensile and that their magnitude increases with scanning speed of laser beam. Kadolkar et al. [20] reported a similar behavior. They used the $\sin^2\Psi$ method to measure surface strain on TiC/Al coating on aluminum substrate. Although they did not assume any rotation of principal stress components towards the laser beam scanning direction, they detected both principal stress components being compressive near the surface, but for higher cooling rates these stresses become less compressive.

The residual stresses were evaluated between the center of the 5th and overlap with the 6th track. These measurements partly overlap each other because the width of the gauge length was fixed to 1.5 mm and the lateral displacement was 1.0 mm.

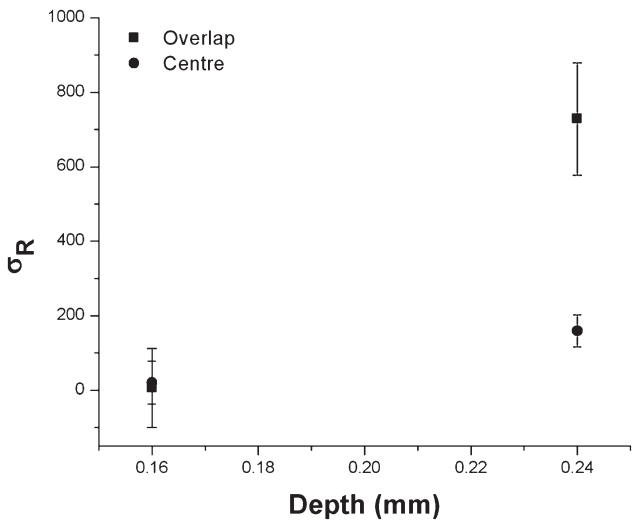

Fig. 10. The residual stresses σ_R calculated with $E_{Co(311)}$ at the centre of the 5th track and its neighboring overlap.

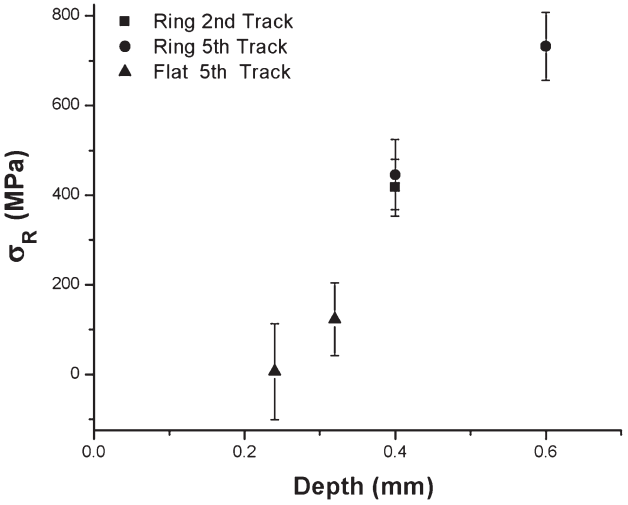

Fig. 11. Residual stresses on: 5th track of the flat cladding; 5th track and 2nd tracks of the round cladding. σ_R's were calculated with $E_{Co(311)}$ and $\nu_{Co(311)}$.

The effect of the overlap is shown in Fig. 10. A tendency is observed for highest residual strains developed at the overlap region and, consequently this region experiences higher tension.

Effects of the shape of the clad on the residual stresses was estimated by making a comparison of the profiles in the intact flat and round substrates deposited with identical processing parameters (see Fig. 11). Since diffraction phenomena took place at different depths it is not possible to compare directly the values of local strains. For that, one may extrapolate the values obtained indicating that the residual stresses attained in the round sample are shifted to higher levels.

It is possible to estimate the strain or stress release by considering the analysis of an intact sample, where $\sigma_R = \sigma_x + \sigma_y$ holds. It is assumed that in a cross-section section sample σ_x is released and only σ_y remains. As the value of ε_z correspond to the local stress state, it is possible to describe the stress tensor

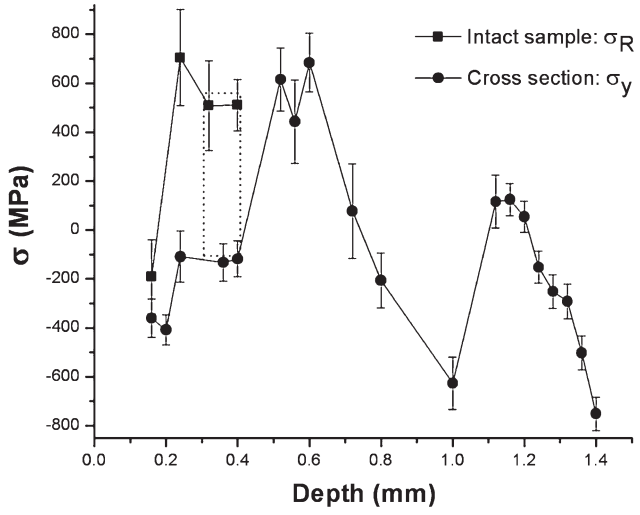

Fig. 12. Residual stresses profile: on intact cladding assuming ε_z function of σ_R. On the cross-section, it is assumed a release of σ_x and ε_z is only function of σ_y. σ is calculated with $E_{Co(311)}$ and $\nu_{Co(311)}$.

when one knows the values of σ_R and σ_y. The analysis of stress plots in an intact and a cross-sectioned cladding is used as illustration (see Fig. 12). The samples were deposited under the same processing conditions and a similar grain distribution is expected. This aspect is reflected on the similarity of the curves profiles measured in reflection and transmission modes indicating that X-ray diffraction took place at equivalent depths on the samples. The values of stress should be compared at similar positions in order to take in consideration possible effects of the depth. However, as aforementioned texture did not allow for diffraction through the whole depth of the clad scanned in reflection mode. The plateau region of the stress curves was chosen for analysis, indicated by the dashed line in Fig. 12. The shift of the curve from tensile to compressive is clear when the cladding is sectioned, indicating the release of positive stresses. The averaged residual stress values in these regions are $\sigma_R = 500$ MPa and $\sigma_y = -100$ MPa, from which we conclude that $\sigma_x = 600$ MPa at that specific depth.

The residual stresses as a function of depth (Fig. 13) and horizontal position (Fig. 14) were measured in transmission mode. The depth profiles were taken from the central, 5th and 8th, i.e. last-but-one track. The central track is found in pure tensile stress state until 0.8 mm depth, it was not possible to analyze the remaining depth due to lack of diffraction. The last-but-one track is under tensile stress until 0.8 mm changing towards the substrate into compression. The horizontal profiles at different depths complemented the previous observations on the 5th and 8th track. The width scanning experiment was conducted under lower counting time than the depth profiles and as consequence the error bars increase. At 0.3 mm depth tensile stress state is found mainly in the central region of the cladding layer, around the 5th track, whereas at the extremities at this depth the compression state dominates. At 0.8 mm one far end of the clad layer is in tensile state, whereas the center and the other far end of the clad are in compression. From 0.3 to 0.8 mm depth the far ends of the curves are shifted towards positive values. Gripenberg at al. [21] used three different

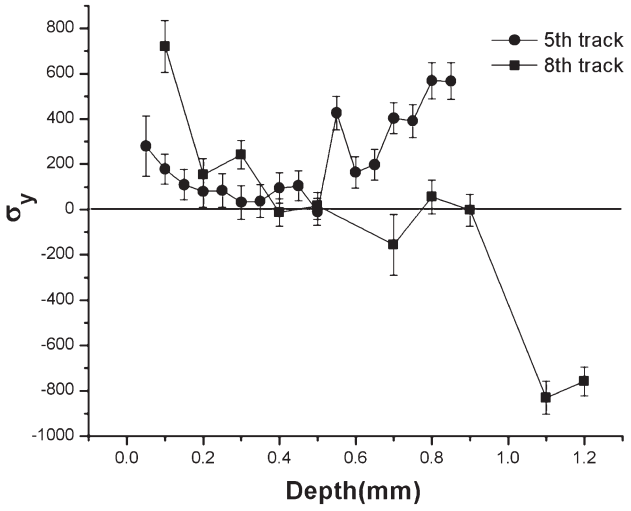

Fig. 13. Profile of residual stress σ_y on cross-sections of 5th and 8th tracks. σ_y is calculated using $E_{Co(311)}$ and $\nu_{Co(311)}$.

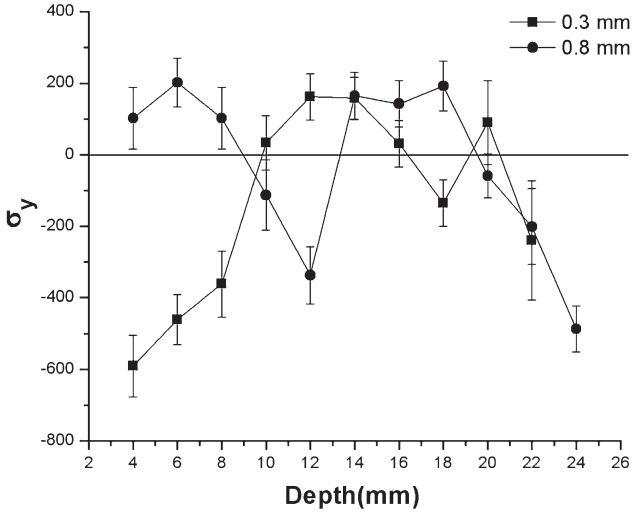

Fig. 14. Horizontal profile of residual stresses σ_y on cross-section, measured at 0.3 and 0.8 mm depths. σ_y's is calculated with $E_{Co(311)}$ and $\nu_{Co(311)}$.

methods to study the residual stress profile in very thick (10 mm) austenitic steel welding clad on a ferritic steel substrate. They detected a clear change from tensile to compressive residual stresses when proceeding from the clad to the base material. Neutron diffraction technique was able to detect significant local fluctuations in residual stresses in the clad material, similar as in our case. Also in [22] it is observed by $\sin^2\Psi$ method that the surface stress distribution after remelting of plain carbon steel is rapidly varying and one should be careful by measuring only average stresses on laser treated surfaces. A longitudinal principal stress component was measured in this experiment 50% larger than transversal one. Pilloz et al. [3] presented a simple phenomenological model for residual stresses induced by laser cladding. They assume that longitudinal and transversal stress components are nearly equal and their variations are small inside the coating but sharp on interfaces between three different zones: coating/heat-affected zone/substrate. Thermal contraction effects in these individual zones during the cooling process determine the sign of residual stresses inside them. The magnitude of the creep inside heat-affected zone also influences sign and level of residual stresses. Results of our measurements show that both assumptions from this model are far from reality and residual stress fields formed inside laser clad and its surrounding are far more complicated.

4. Conclusions

X-ray diffraction techniques were used for the characterization of residual stresses in Co-based laser deposited claddings. From the combination of these observations with microstructural data, phase analysis, nanohardness measurement and calculation of elastic moduli we may draw the following conclusions.

– Relatively large grains and strong texture formed during the laser track solidification do not allow to perform stress

analysis with a synchrotron radiation diffraction through the whole coating depth in the reflection mode.
- Young's modulus calculated for (311) planes in pure γ-Co crystal is about 75% of the value of cobalt based alloy modulus estimated from nanohardness measurements.
- The stress state of the Stellite 20 coating near the surface is biaxial tension, when the major component is much larger than the minor one. The major component is not parallel to the clad direction, but is tilted from this direction about 40°. This behavior is connected with a change of orientation of cooling front during the overlapping of laser tracks in comparison with single laser track cladding.
- The residual stresses usually increases with depth and it may reach the value of yield stress at half of the thickness of the coating. Near the coating/substrate interface the sign of the internal stresses is changed to compression.
- The variation of the stress as a function of depth is not smooth and also its behavior varies from track to track.
- The residual stress increases with scanning speed, track overlapping and change from flat to round shape of the substrate.

Acknowledgements

The authors would like to acknowledge the NIMR/IOP for the financial support and ESRF for the beam line time, especially Beamline ID-31 and Dr. Francois Fauth for the technical support during the experiments and group FAME38 for sample holders and sharing experiment experience.

References

[1] U. de Oliveira, V. Ocelík, J.Th.M. De Hosson, Surf. Coat. Technol. 197 (2005) 127.
[2] R. Vilar, J. Laser Appl. 11 (1999) 64.
[3] M. Pilloz, J.M. Pelletier, A.B. Vannes, J. Mater. Sci. 27 (1992) 1240.
[4] A. Pyzalla, Physica. B 276-278 (2000) 833.
[5] C.T. Sims, N.S. Stoloff, W.C. Hagel, Superalloys II, Willey-Interscience, New York, 1987, p. 575.
[6] W. Voigt, Lehrbuch der kristallphysik, Teubner, Leipzig, 1928.
[7] A. Reuss, Z. Angew, Math. Mech. 9 (1929) 49.
[8] R. Hill, Proc. Phys. Solids 15 (1952) 349.
[9] M.E. Fitzpatrick, A. Lodini, Analysis of Residual Stress by Diffraction using Neutron and Synchrotron Radiation, Taylor and Francis, London, 2003, p. 47.
[10] B. Clausen, T. Lorentzen, T. Leffers, Acta Mater. 46 (1998) 3087.
[11] B. Clausen, T. Lorentzen, T. Leffers, Acta Mater. 51 (2003) 6181.
[12] P. Soderlind, Phys. Rev., B 50 (9) (1994) 5918.
[13] I.C. Nohian, J.B. Cohen, Residual stress measurement by diffraction and evaluation, Ilschner and Grant, Springer-Verlag, New York, Berlin, Heilderberg, 1987, 82–84.
[14] I.C. Nohian, J.B. Cohen, ibid, 117–143.
[15] P.J. Withers, J. Appl. Crystallogr. 37 (2004) 596.
[16] P.J. Withers, J. Appl. Crystallogr. 37 (2004) 607.
[17] A.F.A. Hoadley, M. Rappaz, M. Zimmerman, Metall. Trans., B 22 (1) (1991) 101.
[18] J. Grum, M. Žnidaršič, Mater. Manuf. Process. 19 (2) (2004) 243.
[19] X.B. Zhou, J.Th.M. De Hosson, Scr. Metall. Mater. 25 (1991) 2007.
[20] P. Kadolkar, H. Wang, T.R. Watkins, N.B. Dahotre, Int. J. Adv. Manuf. Technol. 23 (2004) 350.
[21] H. Gripenberg, H. Keinänen, C. Ohms, H. Hänninen, D. Stefanescu, D. Smith, Mat. Sci. Forum 404–407 (2002) 861.
[22] B.A. Van Brussel, H.J. Hegge, J.Th.M. De Hosson, Scr. Metall. Mater. 25 (1991) 779.